11th International Symposium on Turbulence and Shear Flow Phenomena (TSFP11)
Southampton, UK, July 30 to August 2, 2019

FLOW INSTABILITIES IN SHOCK WAVY-WALL INTERACTION

Bowen Yan
Department of Aerospace Engineering
Tsinghua University
Beijing 100084, China
yanbw15@mails.tsinghua.edu.cn

Song Fu
Department of Aerospace Engineering
Tsinghua University
Beijing 100084, China
fs-dem@mail.tsinghua.edu.cn

ABSTRACT

The reflection of a planar shock on a wavy wall is simulated in two-dimensional geometry by using the gas kinetic scheme (GKS). A high-order accurate reconstruction based on minimized dispersion and controllable dissipation (MDCD) is implemented in the second-order accurate GKS to improve the accuracy and resolution.

We have investigated the unsteady flow features for different shock reflection cases. These cases are designed for different Mach numbers with various shapes of the wavy-wall individually. Comparisons with experimental data including mean velocity fields and unsteady flow field are presented in this paper. The triple points, which are spontaneously formed on the shock front, cause a periodic cellular wave pattern similar to that of a cellular detonation. As a result of the interaction between transverse waves and the shedding slip lines, large eddy structures are formed at the crest and trough of the sinusoidal wall. Also, the small eddy structures caused by the Kelvin-Helmholtz instability (KHI) will develop in the shocked gas and interact with the large eddies. The effects of Mach numbers and the wall-shapes on the flow instability are analysed in the present paper.

INTRODUCTION

The interaction of shock waves with reflector surfaces is important for aviation safety and detonation ignition. In this shock induced flow phenomenon, several flow instabilities occur at the same time which may lead to the turbulence regime. Such as the Kelvin-Helmholtz instability (KHI) and Richtmyer-Meshkov instability (RMI). RMI plays an important role in Inertial Confinement Fusion (ICF) and astrophysical fluid dynamics. It is generated when a shock wave refracts through the interface between two materials. Perturbations on the interface grow in size and cause the materials to mix [RICHARD & HOLMES (1999)]. After re-shock, the turbulent mixing layer develops rapidly. Besides, there will be wave patterns caused by the reflected shock. These patterns, often called "cellular pattern", become obvious when the density ratio is large enough, and the interface is just like the wavy-wall reflector. At the mean time, the KHI is often considered as the secondary small-scale turbulent mixing phenomenon Rikanati *et al.* (2006). Several theories and numerical research [Lodato *et al.* (2016), Lodato & L. Vervisch (2017)] have been conducted on small amplitude wavy-wall shock reflection, and compared with the experiments [Denet *et al.* (2015)]. Under this condition, they have proved that the flow pattern is governed by the motion of triple points, and the viscosity has little influence on the post-shock flow feature. Meanwhile, the shock Mach number is a key factor. Also, there are many studies about the complex flow features after shock reflection from parabolic and cylindrical surface [Shadloo *et al.* (2014)].

In this study, direct numerical simulations using GKS are carried out to investigate the flow instabilities in two dimensional shock reflection cases. These cases are designed for various shapes of the wavy-wall with different Mach numbers. Comparisons with experimental data and among different cases including the re-shock case are presented at different time. Also, the origin and development of the instabilities of slip lines are analysed.

NUMERICAL METHODS

Gas Kinetic Scheme

GKS is based on a time-dependent evolution solution of the Bhatnagar-Gross-Krook (BGK) model for Boltzmann equation, and targeting on the numerical solution of the compressible Navier-Stokes equations Xu (2001). The 3D BGK equation can be written as:

$$\frac{\partial f}{\partial t} + \boldsymbol{u} \cdot \frac{\partial f}{\partial \boldsymbol{x}} = \frac{g - f}{\tau} \tag{1}$$

where f is the gas distribution function and g is the equilibrium state approached by f. Both f and g are functions of space $\boldsymbol{x}(x_1, x_2, x_3)$ time t, particle velocities $\boldsymbol{u}(u, v, w)$, and internal variable $\boldsymbol{\xi}$. The relationship between the particle collision time τ and viscosity can be written as $\tau = \mu/p$.

The equilibrium state is a Maxwellian distribution:

$$g = \rho\left(\frac{\lambda}{\pi}\right)^{\frac{K+3}{2}} \mathrm{e}^{-\lambda\left[(\boldsymbol{u}-\boldsymbol{U})^2+\boldsymbol{\xi}^2\right]} \tag{2}$$

where ρ is the density, $\boldsymbol{U}(U,V,W)$, are the macroscopic velocities, internal variable $\xi^2 = \xi_1^2 + \cdots + \xi_K^2$, $K = (5-3\gamma)/(\gamma-1)$ is the total number of degrees of freedom, γ is the ratio of specific heat , and $\lambda = 1/(2RT)$, R is the universal gas constants, and T is the temperature. The general time-dependent solution of f can be obtained as:

$$f(\boldsymbol{x},t,\boldsymbol{u},\boldsymbol{\xi}) = \frac{1}{\tau}\int_0^t g\left(\boldsymbol{x}',t',\boldsymbol{u},\boldsymbol{\xi}\right)\mathrm{e}^{-(t-t')/\tau}\mathrm{d}t' + \mathrm{e}^{-t/\tau} f_0(\boldsymbol{x}-\boldsymbol{u}t) \tag{3}$$

where f_0 is the initial gas distribution at beginning of each time step, and $\boldsymbol{x}' = \boldsymbol{x} - \boldsymbol{u}\,(t-t')$ is the particle trajectory.

In order to update the macroscopic flow variables, the finite-volume method (FVM) is used:

$$\boldsymbol{Q}_{ijk}^{n+1} = \boldsymbol{Q}_{ijk}^{n} + \frac{1}{V_{ijk}}\oiint_{S_{ijk}}\int_{t^n}^{t^n+\Delta t} F\mathrm{d}t\mathrm{d}S \tag{4}$$

where $\boldsymbol{Q}$ denotes the macroscopic conserved quantities, and $\boldsymbol{F}$ is the numerical flux. Their relationship with the gas distribution function:

$$Q = (\rho \quad \rho\boldsymbol{U} \quad \rho E)^{\mathrm{T}} = \int f\boldsymbol{\psi}\mathrm{d}\Xi \tag{5}$$

$$\boldsymbol{F}_m = \int u_m f\boldsymbol{\psi}\mathrm{d}\Xi \tag{6}$$

where $\boldsymbol{\psi}$ is the component of the vector of moments

$$\boldsymbol{\psi} = (\psi_1,\psi_2,\psi_3,\psi_4,\psi_5)^T = \left(1,u,v,w,\frac{1}{2}\left(u^2+v^2+w^2+\xi^2\right)\right)^T \tag{7}$$

and $d\Xi = dudvdwd\xi$ is the volume element in the phase space with $d\xi = d\xi_1 d\xi_2 \cdots d\xi_K$.

The two unknowns g and f_0 must be specified to get the gas distribution function f .In order to target on the NS solution, the first order of Chapman-Enskog expansion gives the form (For example , along the normal direction x_1 of the interface):

$$\begin{aligned} f_0(\mathbf{x},\mathbf{u},\xi) &= \left(1 + a_m^l x_m - \tau\left(a_m^l u_m + A^l\right)\right)(1-\mathrm{H}[x_1])\,g^l \\ &\quad + \left(1 + a_m^r x_m - \tau\left(a_m^r u_m + A^r\right)\right)\mathrm{H}[x_1]\,g^r \\ g(\mathbf{x},t,\mathbf{u},\xi) &= \left(1 + (1-\mathrm{H}[x_1])\,\overline{a}_m^l x_m + \mathrm{H}[x_1]\,\overline{a}_m^r x_m + \overline{A}t\right)g_0 \end{aligned} \tag{8}$$

where H[x] is the Heaviside function, g_0 is a local Maxwellian distribution function located at interface ($x_1 = 0$), the symbol 'l' or 'r' means the left or right side of the cell interface, a and A correspond to the spatial and temporal derivatives of the distribution function:

$$\begin{aligned} a &= a_\alpha\psi_\alpha = (\partial g/\partial x)/g \\ A &= A_\alpha\psi_\alpha = (\partial g/\partial t)/g \end{aligned} \tag{9}$$

Just like the traditional FVM schemes, FV-GKS is also composed of an initial reconstruction stage followed by a dynamical evolution stage. In the reconstruction stage, we use the second order MUSCL interpolation with van Leer limiter, the flow variable $\boldsymbol{Q}$ is distributed linearly in cell j:

$$\boldsymbol{Q}_j(x) = \overline{\boldsymbol{Q}}_j + L(s_+,s_-)\left(x - x_j\right) \tag{10}$$

where the $\overline{\boldsymbol{Q}}$ is the cell averaged conservative variable, their differences between neighbouring cells $s_+ = \left(\overline{\boldsymbol{Q}}_{j+1} - \overline{\boldsymbol{Q}}_j\right)/\Delta x$ and $s_- = \left(\overline{\boldsymbol{Q}}_j - \overline{\boldsymbol{Q}}_{j-1}\right)/\Delta x$, the slop of $\overline{\boldsymbol{Q}}$ in cell j is constructed as

$$L(s_+,s_-) = (s_+,s_-)\,\frac{|s_+||s_-|}{|s_+|+|s_-|} \tag{11}$$

where $S(s_+,s_-) = \mathrm{sign}(s_+) + \mathrm{sign}(s_-)$.

With the distribution of $\boldsymbol{Q}$ and the relationship in Eq.(4) and Eq.(9), we can determining a in Eq.(8) . Since mass, momentum, and energy are conserved during particle collisions, we can get the conservation constraint to determining A :

$$\int \psi(au + A)g\mathrm{d}\Xi = \mathbf{0} \tag{12}$$

Then we get the final explicit form of f:

$$\begin{aligned} f(\mathbf{0},t,\mathbf{u},\xi) &= (1-C_0)\,g_0 + (t - \tau + C_1)\,\overline{A}g_0 \\ &\quad + (-\tau + C_1 + C_2)\left(\overline{a}_m^l u_m \mathrm{H}[u_1] + \overline{a}_m^r u_m\,(1-\mathrm{H}[u_1])\right)g_0 \\ &\quad + \left(C_0 - (C_1+C_2)\,a_m^l u_m - C_1 A^l\right)\mathrm{H}[u_1]\,g^l \\ &\quad + (C_0 - (C_1+C_2)\,a_m^r u_m - C_1 A^r)\,(1-\mathrm{H}[u_1])\,g^r \end{aligned} \tag{13}$$

where $C_0 = \mathrm{e}^{-t/\tau}$, $C_1 = \tau C_0$, $C_2 = tC_0$. With the Eq.(5) we can get the numerical flux, and update the $\boldsymbol{Q}$ using Eq.(3)

Additionally, in order to collocate with curvilinear grid, we transform the the irregular physical space (x,y,z) into a regular computational space (ε,η,ζ). Using the geometric information of each finite volume gird to calculate the coordinate transformation coefficients, we can obtain all the derivatives in the computational domain.

The nonequilibrium gas distribution function in GKS proposes a unified physical dissipation mechanism, which involves the statistical law of the free motion and collision of molecules. Benefit from this, GKS can accurately capture the evolution of shock structures without any additional means of diagnosing or treating Li *et al.* (2005). Besides, a high-order accurate reconstruction based on MDCD is implemented in the second-order accurate GKS to improve the accuracy and resolution.

Problem setup

According to the experimental data Denet *et al.* (2015), the physical domain for the simulations considered in this paper is 10cm in the streamwise direction (denoted as x) and 2cm in the transverse directions (denoted as y), shown in fig.1. A grid sensitivity study using 1024×512, 2048×1024, and 4096×2048 meshes shows that the most relevant flow features are well captured with the medium grid whose spatial resolution is about 20 μm. A plane shock wave propagating from right to left is initially located at x = 8.0 cm. The right boundary is set as an inflow, whose parameters

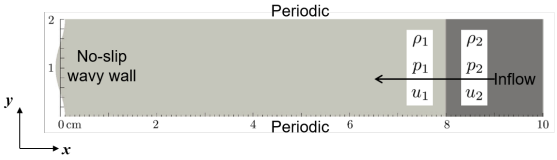

Figure 1: Computation domain schematic

correspond to the compressed state of the incident shock. Given the incident shock Mach number (M_1), the post-shock parameters can be determined according to the Rankine-Hugoniot relationships. We have investigated the flow with different, and the flow parameters of M_1=1.5 are set to match the experiment of Denet *et al.* (2015) and the work of Lodato *et al.* (2016), and shown in Table1. The top and bottom boundaries are periodic. As for the no-slip wall profile is chosen as $f(y)$, and the incident angle of shock θ_w can be obtained as:

$$\begin{cases} f(y) = A_w \cos(2\pi y/\lambda_w) \\ \theta_w = 90^\circ + (180^\circ/\pi)\tan^{-1}[-2\pi\chi\sin(2\pi y/\lambda_w)] \end{cases} \quad (14)$$

where χ is the shape parameter of the wall (ratio of amplitude to wavelength), and Table.1 shows a case of $\chi = 0.05$.

Table 1: Initial flow conditions.

Item	Symbol	Value
Domain size	$L_x \times L_y$	10.0 × 2.0 cm
Number of elements	$N_x \times N_y$	2000 × 1000
Wavy-wall amplitude	A_w	1.0 mm
Wavy-wall wavelength	λ_w	2.0 cm
Incident shock Mach	M_1	1.5
Incident shock speed	u_i	-514 m/s
Initial speed	u_1	0.0 m/s
	u_2	-237.96 m/s
Initial density	ρ_1	1.208 kg/m^3
	ρ_2	2.25 kg/m^3
Initial pressure	p_1	101 325.0 Pa
	p_2	249 090.6 Pa
Viscosity (at 291.15 K)	μ_0	1.827 ×10^{-5} kg/(m·s)

RESULTS AND DISCUSSION

In order to investigate the effects of different factors on the flow instability, cases with for different incident Mach numbers (M_1 = 1.5, 3.0, 4.3, 5.0) and different wall shapes (χ = 0.05, 0.1, 0.17, 0.32) are performed respectively. Firstly, the basic flow field is analyzed for the benchmark case (M_1 = 1.5; χ = 0.05) and compared with the experimental results. Most instantaneous flow structures are shown in numerical Schlieren images at M_1 = 3.0, where the images of slip line have the best display effect. And detailed analysis are given to explain the mechanics of the slip line instability. Then, the comparison between different flow cases are discussed and show us the effects of incident Mach number and wall shapes on the various flow instabilities.

Verification of results

As we can see from the fig.2, Due to the small amplitude of the wavy-wall, the reflection is regular and there is no transition to Mach reflection during the whole interaction between the incident shock and the wall. But the reflected shock front appears to have a smoothly curved profile just after reflection. The triple points will form spontaneously when the saddle points move to the shock front. And we can

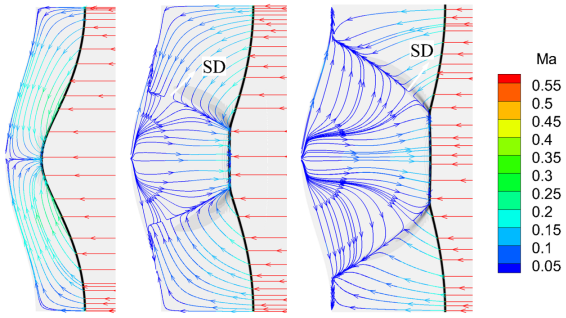

Figure 2: Streamline at 10 μs, 20 μs, 25 μs after reflection, Coloured by the local Mach number

calculate the transverse velocity u_T of the triple points, and the angle between the horizontal and the normal oriented in the opposite direction to propagation α_n shown in fig.3. The quantitative comparison of u_T and α_n with the experimental data is shown in Table2.

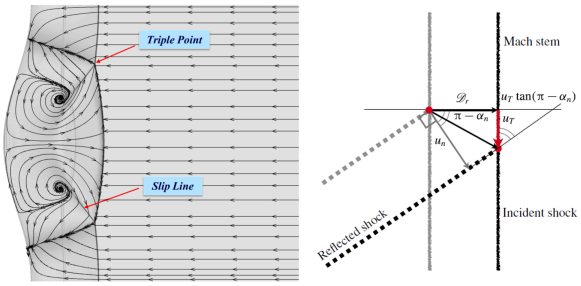

Figure 3: Streamline and the triple point, Geometrical construction of the transverse wave front

Table 2: Comparison to experiments.
(u_T is the transverse velocity of triple point
α_n is the angle between reflect shock and Mach stem)

	Exp	GKS	error
u_T	310	310±3	±1%
α_n	133.7	137.4±2	2~5%

Also, a qualitative comparison of the simulated Density gradient magnitude with the experimental schlierens is given in fig.4. The results are presented at the instants of 120

μs and 200 μs after after reflected from the wall. The comparison is quite satisfactory.

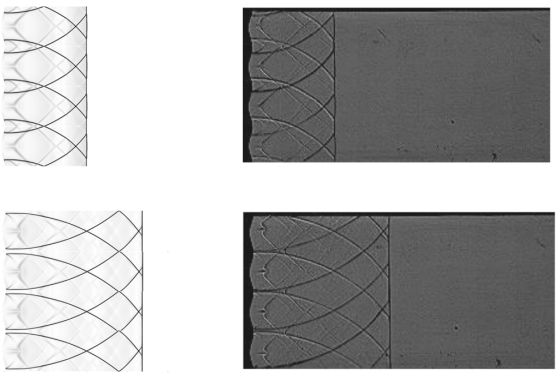

Figure 4: Comparison with the experiment, $M_1 = 1.5$.

Instantaneous flow features

The main flow structures are like a cellular pattern caused by the motions of triple points and the waves. Results are shown at both early fig.3 and late time fig.13 after the shock reflection. As the typical three-shock configuration in the Mach reflection presented in textbooks COURANT & FRIEDRICHS (1948). The triple points observed on the cellular shock wave is constituted by four lines ending at the same point: an incident shock (IS), a reflected shock (RS), another shock called a Mach stem (MS) and a slip line (SL), which is located in the portion of gas between the Mach stem and the reflected shock. A pair of the spontaneously formed triple points moves along the shock front in opposite direction, causing the transverse waves travelling among the post shock flow field. After each collision of the triple points, the slip line will shed and encounter at the crests and troughs. The large scale vortex is formed when the slip line encounters and interacts with each other, shown in Fig.5. In the late time as shown in Fig.6, the unstable flow field will be shocked again. And after the re-shock process, the instabilities develop into the turbulence regime quickly.

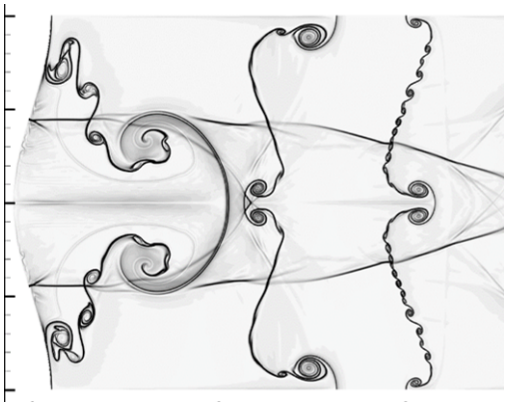

Figure 5: Density gradient magnitude, at 112 μs after reflected from the wall.

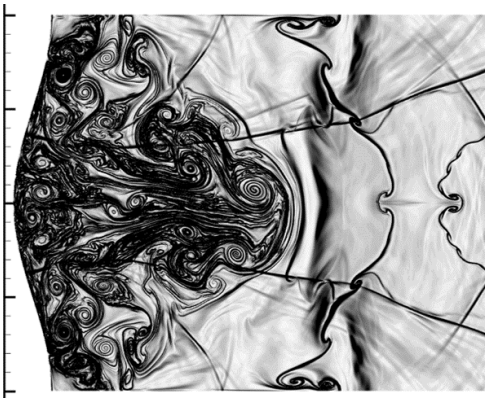

Figure 6: Density gradient magnitude, 364 μs (the re-shock already happened).

Slip line instability

As we can see in the instantaneous flow Fig.5, there are obvious slip line instabilities happened both in large-scale and small-scale. When the shed slip lines encounter at the crests and troughs, there will be a jet flow between the two structures because of the symmetry. The mushroom-like unstable structures appear under the RM instability mechanics. On the other hand, under the action of the molecular viscosity, the slip line is transformed into a thin shear layer, far away from the encounter point, shown as Fig.7. In the

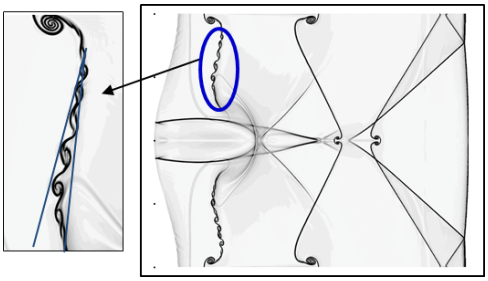

Figure 7: The thin shear layer on the slip line.

work of Rikanati *et al.* (2006), this slip-stream instability is described as a secondary small-scale turbulent mixing phenomenon. The growth rates of the large-scale Kelvin-Helmholtz shear flow instability can be used to model the evolution of the slip-stream instability in ideal gas. We can also see the fusion of small vortex in the shear layer in Fig.8, which indicates small-scale instability of the slip line is dominated by the Kelvin-Helmholtz instability Wan *et al.* (2017).

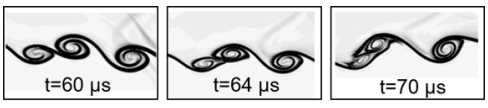

Figure 8: Merger of the small vortex.

Effects of the Mach number and wall shapes

In order to investigate the influence of the wall shapes on the flow instability, shock reflections on different wavy wall are simulated at high Mach number cases (M_1 = 3.0, 4.3, 5.0). According to the smallest value of θ_w , different reflection types may occur at specific Mach number [G.Ben-Dor. (2007)], including Regular reflection (RR), Double-Mach reflection (DMR), Transitional-Mach reflection (TMR), Single-Mach reflection (SMR) (Fig. 9). Four

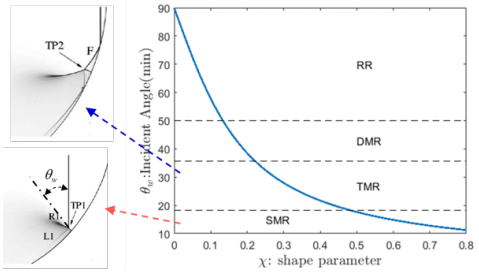

Figure 9: Different reflection types with the change of χ, at M_1 = 3.0.

different wall shapes are simulated correspond to the four reflection types receptively, as shown in Fig.10. For the deep cavity wall shapes, shock focusing occurs with a jet flow. We have also compared the scaled jet velocity between two

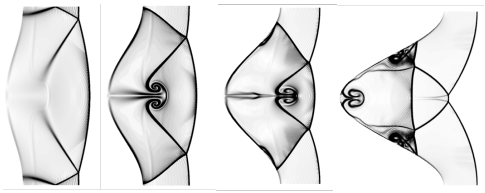

Figure 10: Density gradient magnitude at 10 μs after reflection (χ = 0.05, 0.1, 0.17, 0.32), M_1 = 3.0

typical wall shapes (χ = 0.17 and Cylindrical surface) at different high Mach numbers in fig. 12.

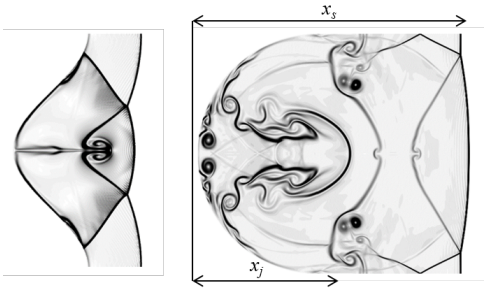

Figure 11: Diagram of the dimensionless speed

In three dimensional experiments, [Shtemenko & Shugaev (1997)] pointed out that if the Reynolds number is equal to 2-3e5, and the Mach number is equal to 4.3-5, the instability of vortices at the end of the jet may cause

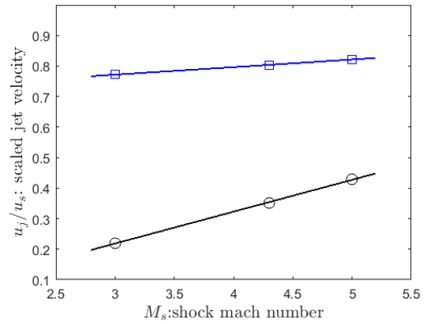

Figure 12: velocity of the primary jet scaled by the speed of shock front, as a function of Mach number. Circle: Cylinder surface; Square: Sinusoidal surface χ=0.17

a disturbance on the shock front. Because of the resonant excitation of vortices, the flow inside the cylinder cavity becomes turbulent. But we haven't found this phenomenon at the same condition in two-dimensional flow. Thus a 3D simulation is what we expect to do next.

CONCLUSIONS

In our simulation of the high Mach number shock wavy-wall reflection, we found that the small-scaled instability of the vortices formed on slip-lines is governed by Kelvin-Helmholtz mechanism and the interaction with transverse waves. whereas, the large-scaled one is caused by the encounters of the slip line, and under the RM instability mechanism.

After the study of the wall shape effect on the flow instability, it can be find that for the sinusoidal wall shapes, the range χ =0.13-0.21 is shown to be easier for excitation instability, where the jet is even stronger than the two-dimensional cylinder surface case. For all deep cavity wall shapes, shock focusing occurs with a jet flow, whose scaled velocity is linearly dependent on the incident shock Mach number. And the jet influences the stability of the post-shock flow.

Even though there are some studies show that disturbances at the shock front occur under appropriate conditions. However, two-dimensional cases have some inhibition effects on the development of instabilities of the jet and the shock front. As an outlook, three-dimensional simulations including boundary-layer effects will be carried out on.

ACKNOWLEDGEMENTS

This work was supported by Science Challenge Project (No. TZ2016001). Computational resources were provided by the High Performance Computing Center at Tsinghua University and the Sunway TaihuLight Super Computing Center. The authors also acknowledge technical discussion with Prof. Qibing Li at Tsinghua University.

REFERENCES

COURANT, R. & FRIEDRICHS, K. O. 1948 Supersonic flow and shock waves. *Springer Verlag* .

Denet, B., Biamino, L., Lodato, G., Vervisch, L. & Clavin., P. 2015 Model equation for the dynamics of wrinkled shockwaves: Comparison with dns and experiments. *Combustion Science and Technology* **187**, 296–323.

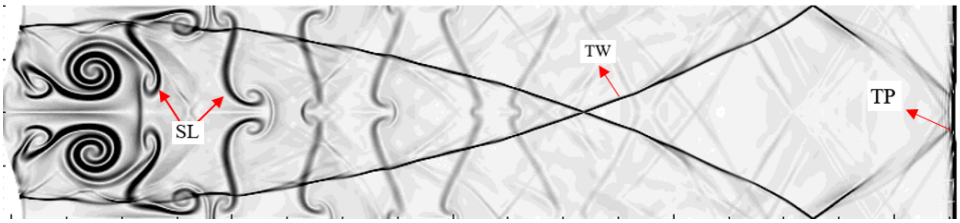

Figure 13: Density gradient magnitude at 100 μs (M_1 = 3.0, χ=0.05);
SL, slip line; TP, triple point; TW, transverse wave

G.Ben-Dor. 2007 Shock wave reflection phenomena. *Springer Verlag* .

Li, Q, Fu, S & Xu, K. 2005 A compressible navier-stokes flow solver with scalar transport. *Journal of Computational Physics* **204(2)**, 692–714.

Lodato, G. & L. Vervisch, P. Clavin. 2017 Numerical study of smoothly perturbed shocks in the newtonian limit. *Flow Turbulence Combust* **99**, 887–908.

Lodato, G., Vervisch, L. & Clavin., P. 2016 Direct numerical simulation of shock wavy-wall interaction: analysis of cellular shock structures and flow patterns. *J. Fluid Mech* **789**, 221–258.

RICHARD & HOLMES 1999 Richtmyer-meshkov instability growth: experiment, simulation and theory. *J. Fluid Mech* **389**, 55–79.

Rikanati, O, Sadot, G, Ben-Dor, D, Shvarts, T, Kuribayashi & K., Takayama 2006 Shock-wave mach-reflection slip-stream instability: a secondary small-scale turbulent mixing phenomenon. *Phys Rev Lett* **96**.

Shadloo, M. S., Hadjadj, A. & Chaudhuri., A. 2014 On the onset of postshock flow instabilities over concave surfaces. *PHYSICS OF FLUIDS* **26**, 296–323.

Shtemenko & Shugaev 1997 Propagation and reflection of shock waves. *Series on Advances in Mathematics for Applied Sciences* **49**.

Wan, W. C., Malamud, G., Shimony, A., Di Stefano, C. A., Trantham, M. R., Klein, S. R., Shvarts, D., Drake, R. P. & Kuranz, C. C. 2017 Observation of dual-mode, kelvin-helmholtz instability vortex merger in a compressible flow. *Physics of Plasmas* **24** (5), 055705.

Xu, Kun 2001 A gas-kinetic bgk scheme for the navier–stokes equations and its connection with artificial dissipation and godunov method. *Journal of Computational Physics* **171** (1), 289–335.